physica status solidi b
www.pss-b.com

Modeling the Influence of Deposition Parameters on the Crystalline Degree in the Simulation of Polycrystalline Silicon

Mikael Santonen, Antti Lahti, Divya Srivastava, Zahra Jahanshah Rad, Mikko Miettinen, Masoud Ebrahimzadeh, Johanna Laaksonen, Pekka Laukkanen, Marko Punkkinen, Kalevi Kokko, Antti Kuronen, Katja Parkkinen, and Markus Eklund*

Polycrystalline silicon (poly-Si) has been and still is a pivotal material, particularly in the electronics and solar energy industries. Controlling crystallization is one of the challenges, e.g., in producing poly-Si films for radio frequency applications. Since film growth by deposition is a random process, producing a specific grain size distribution for poly-Si is challenging. By combining molecular dynamics simulation data with surface diffusion physics, novel transparent models are constructed that shed light on the physics behind the deposition of poly-Si thin films and assist the selection of simulation parameters. Both probabilistic and geometric approaches are used to find relevant simulation parameters and their bounds to describe the complex grain–grain boundary interactions in the growth of poly-Si thin films. Poly-Si growth simulations provide valuable information to better understand the features of optimal growth conditions. The constructed parameterized deposition model is fitted to the simulation data. In addition to further refining the simulation of customized poly-Si films, the presented modeling concept can also be used more generally in the analysis of physical vapor deposition.

1. Introduction

Poly-Si is used in many modern technology applications, for example, in microelectronics devices such as metal-oxide-semiconductor field-effect transistors, in photovoltaic and photonics devices like solar cells, in microelectromechanical systems, thin film transistors, in displays, sensors, and actuators, and in low-loss coatings of Si wafers in radio frequency (RF) applications,[1–8] and future applications such as integrated poly-silicon avalanche mode light-emitting device[9] and gate-all-around transistors.[10] Poly-Si is also a good choice in terms of sustainable development because it is recyclable and nontoxic. Moreover, Si is the second most abundant element in the Earth's crust.

Like in single-crystal Si, the doping affects the electrical properties of poly-Si. However, poly-Si has another complementary engineering parameter that affects its electrical, optical, and mechanical properties: grain size, which is highly dependent on the deposition conditions. The grain size typically increases as the annealing time increases. Controlling the grain size of poly-Si is an active area of research.[8,11–13] Through the crystallization methods, an engineer can control the size of the grains in poly-Si and vary the physical properties of poly-Si.

Amorphous Si (a-Si) is deposited, e.g., using physical vapor deposition, chemical vapor deposition (CVD), plasma-enhanced CVD, very high-frequency CVD, and magnetron evaporation. a-Si can be used in the same applications as poly-Si unless the lower mobility of charge carriers of a-Si poses obstacles. Low-pressure CVD is the most popular method for depositing polysilicon films. There are two general types of manufacturing methods for poly-Si, to deposit the poly-Si from the beginning or to deposit the a-Si and then annealing the a-Si for crystallization.[10] Various methods such as laser-annealed crystallization,[12,14] metal-induced crystallization,[15,16] and solid-phase crystallization[17–19] have been used to obtain high-quality poly-Si films. Large amounts of poly-Si are produced using the Siemens process (solar cells and electronics) and the fluidized bed reactor (granular poly-Si).

M. Santonen, A. Lahti, D. Srivastava, Z. Jahanshah Rad, M. Miettinen, M. Ebrahimzadeh, J. Laaksonen, P. Laukkanen, M. Punkkinen, K. Kokko
Department of Physics and Astronomy
University of Turku
FI-20014 Turku, Finland
E-mail: kalevi.kokko@utu.fi

A. Kuronen
Department of Physics
University of Helsinki
P.O. Box 43, FI-00014 Helsinki, Finland

K. Parkkinen, M. Eklund
Okmetic Oyj
PL 44, 01301 Vantaa, Finland

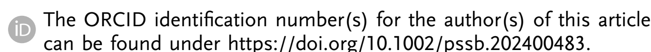
The ORCID identification number(s) for the author(s) of this article can be found under https://doi.org/10.1002/pssb.202400483.

© 2024 The Author(s). physica status solidi (b) basic solid state physics published by Wiley-VCH GmbH. This is an open access article under the terms of the Creative Commons Attribution License, which permits use, distribution and reproduction in any medium, provided the original work is properly cited.

DOI: 10.1002/pssb.202400483

15213951, 0, Downloaded from https://onlinelibrary.wiley.com/doi/10.1002/pssb.202400483 by Duodecim Medical Publications Ltd, Wiley Online Library on [17/01/2025]. See the Terms and Conditions (https://onlinelibrary.wiley.com/terms-and-conditions) on Wiley Online Library for rules of use; OA articles are governed by the applicable Creative Commons License

The charge carrier mobility is greatly improved due to the increased grain size because a large grain size means fewer grain boundaries and thus reduced charge carrier scattering from the grain boundaries.[20] On the other hand, there are application areas in which high resistivity is a bonus instead of high conductivity. For instance, silicon substrates of microelectronics applications operating in the RF range suffer from losses and nonlinear behavior due to parasitic conductivity in the substrate. A thin poly-Si layer with a small grain size with more grain boundaries, inserted between the substrate and the device, improves device performance.[21–23] Developing poly-Si films to mitigate parasitic conductivity in RF applications is one of the motivations of the present study.

Grain size affects the absorption coefficient of polycrystalline thin-film materials because the grain boundaries serve as light-scattering centers. Microcrystalline films show effective absorption coefficients up to an order of magnitude higher than monocrystalline silicon at photon energies above 1 eV.[24]

Poly-Si films fabricated on glass or plastic substrates have attracted much attention because of their applications in electro-optical devices. The reason is that the charge carrier mobility of the poly-Si thin film is 10–100 times greater than that of the a-Si thin film. The performance of devices made of poly-Si strongly depends on the grain size since grain boundaries act as traps and recombination centers for charge carriers.[20]

We investigate in this work the deposition conditions of simulations leading to poly-Si films with a certain polycrystalline ratio. The polycrystalline ratio is defined in this work as the ratio of the volume of the crystalline phase to the total volume of poly-Si. We use data from our previous work.[25] By analyzing the deposition process, the deposition model is constructed and fitted to the data. Then the model parameters are given a physical interpretation, which forms a link between the micro- and macroscale silicon.

Our current research is closely related to the effort to increase the performance of poly-Si to improve the properties of substrates for RF microelectronics components. The effect of poly-Si in these applications is to inhibit parasitic surface currents in the substrates, reducing harmful energy losses, cross talk, and nonharmonic distortions. The beneficial effect of poly-Si in these applications is due to the electronic trap states formed in the grain boundaries to trap the mobile parasitic charge carriers. The ability to trap the charge carriers is therefore directly related to the ratio of the volumes of the crystalline grains and noncrystalline grain boundaries. In the present work, we focus on the polycrystalline ratio of poly-Si. A lower polycrystalline ratio is better for the performance of poly-Si substrate in RF applications. Specifically, the aim of the present study is to shed more light on the deposition process of poly-Si and provide guidance for choosing the optimal parameters for efficient simulations of poly-Si deposition.

Our previous studies on poly-Si[25,26] focused on simulating the deposition of poly-Si using classical molecular dynamics and analyzing the obtained films. These investigations covered phenomena ranging from the Ångström scale to the 0.1 μm scale. We explored the impact of growth temperature on grain structure and grain boundaries, as well as the interaction and stability of seed crystallites during the transition from isolated crystallites to poly-Si growth. Additionally, we examined grain size and orientation, grain boundary thickness quantization, and the density of miscoordinated atoms. However, the role of atomic interactions in relation to the simulation conditions was not addressed in these earlier studies. The current work fills this gap by providing an explanation for the highly nonlinear trend observed in the polycrystalline fraction of the simulated films as a function of simulation parameters, including cell size and deposition rate. Furthermore, our work offers valuable guidelines for designing the computer simulations of polycrystalline material deposition.

With the help of physical data fitting, it is possible not only to expand the area of use of the data itself but also to reveal the underlying physics of phenomena and processes related to certain data. Even more valuable connections to basic physical principles can be obtained if a working physical model is constructed based on the data. The development of the physical model is the core of the research discussed next. It opens up possibilities to use the fitted model also for studying other similar systems and phenomena. The physical interpretation of the fitting parameters is useful for the optimization of the deposition conditions of poly-Si films. Furthermore, conducting a similar analysis across a range of deposition temperatures and rates could yield valuable operational guidelines applicable to real-world physical vapor deposition processes. By extending the corresponding analysis to the growth of multicomponent films, it is possible to gain additional insight into, e.g., molecular beam epitaxy and the deposition of III–V semiconductors on silicon.

The article is organized as follows. The Methods of Simulations first presents the most relevant information related to the simulations and analysis of the deposition of poly-Si films done in ref. [25], followed by a description of the construction of the deposition model. In Section 3, the deposition model is constructed and used to fit the deposition simulation data obtained in ref. [25]. Section 4 details the physical interpretation of the model and its parameters. The conclusions are presented in Section 5.

2. Methods of Simulations

The simulation data of poly-Si film depositions are taken from our previous work.[25] The simulations were done using the Large-scale Atomic/Molecular Massively Parallel Simulator (LAMMPS).[27] The interatomic potential used in LAMMPS was chosen based on the test simulations for the lattice parameter, the elastic constants, and the melting temperature of Si. Stillinger–Weber,[28] Tersoff, and two modified Tersoff,[29–31] environment-dependent interatomic,[32] two modified embedded atom method,[33,34] and spectral neighbor analysis[35] potentials were tested. The Stillinger–Weber potential (Equation (1)–(3)) was found to perform best for our project.

$$V = \varepsilon A\left[\sum_{(ij)} v_{ij}^{(2)}(r_{ij}) + \frac{\lambda}{A}\sum_{(ijk)} v_{ijk}^{(3)}(\mathbf{r}_{ij}, \mathbf{r}_{ik})\right] \tag{1}$$

$$v_{ij}^{(2)}(r_{ij}) = \left[B\left(\frac{r_{ij}}{\sigma}\right)^{-p} - 1\right]\exp\left(\frac{1}{r_{ij}/\sigma - a}\right)\Theta(a - r_{ij}/\sigma) \tag{2}$$

© 2024 The Author(s). physica status solidi (b) basic solid state physics published by Wiley-VCH GmbH

physica status solidi b
www.pss-b.com

$$v_{ijk}^{(3)}(\mathbf{r}_{ij}, \mathbf{r}_{ik}) = \exp\left[\frac{\gamma}{r_{ij}/\sigma - a} + \frac{\gamma}{r_{ik}/\sigma - a}\right] \left(\cos(\theta_{jik}) - \cos(\theta^0)\right)\Theta(a - r_{ij}/\sigma)\Theta(a - r_{ik}/\sigma) \tag{3}$$

where $v_{ij}^{(2)}(r_{ij})$ and $v_{ijk}^{(3)}(\mathbf{r}_{ij}, \mathbf{r}_{ik})$ are the two and three body terms, respectively. Θ is the Heaviside step function and $\theta^0 = \arccos(-1/3)$ is the tetrahedral angle. The parameters are given in **Table 1**.

Simulation cells were rectangular parallelepipeds with a square base and sides from 5 to 10 nm and height from 20 to 30 nm (max 200 000 atoms). The substrate of the depositions was a poly-Si layer generated using the Atomsk program[36] and relaxed using LAMMPS. The number of deposited Si atoms is over 80% of the total number of atoms corresponding to about 20 nm thick Si films. At the sides of the simulation cell, periodic boundary conditions were used, whereas fixed boundary conditions were used at the bottom and the top of the cell.

The microcanonical (NVE) thermodynamical ensemble was used in the critical parts of the simulations. The data used in the present study were obtained by adjusting the thermostat (Langevin) at 900 K and the speed of the injected Si atoms was 5 nm ps^{-1} perpendicular to the film surface. The direction of the velocity of the depositing atoms is slightly randomized by selecting the velocity component parallel to the substrate surface randomly within the range (−0.005, 0.005 nm ps^{-1}) for both x- and y-directions.

Since the polycrystalline ratio also depends on temperature, we refer to it here for completeness. The effect of temperature was studied at temperatures from 600 to 1450 K with 25 K steps using 36 nm^2 × 20 nm simulation cell and a deposition period of 250 fs. The polycrystalline ratio (in %) changes with temperature according to Equation (4) (see also **Figure 1**):

$$r_{\text{pc}} = -7.96 \times 10^{-5}(T/K)^2 + 0.179(T/K) - 7.46 \tag{4}$$

More details of the properties of the simulated poly-Si films can be found in refs. [25,26]. In the present work, the noncrystalline parts of the films (top and bottom) are cut out and only the polycrystalline parts are considered. We analyze the structures of the poly-Si films using the polyhedral template matching (PTM) algorithm of OVITO visualization package.[37,38] Data fittings are done using the curve_fit function from Python SciPy library.[39]

Table 1. Stillinger–Weber potential parameters.

Parameter	Value
ε [eV]	2.1683
A	7.049556277
B	0.6022245584
σ [Å]	2.0951
p	4
a	1.80
λ	21.0
γ	1.20

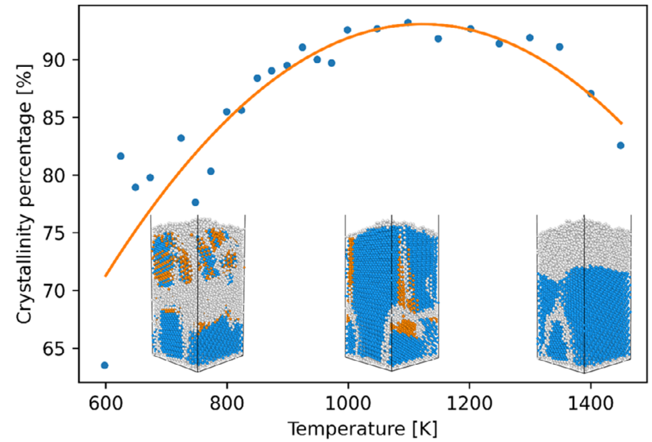

Figure 1. In addition to the deposition parameters, the polycrystalline ratio is also affected by the growth temperature. The second-order curve is a guide for the eye. Three examples of the simulation cells of the deposited poly-Si films are also shown. Their position on the horizontal axis refers to their deposition temperature. The colored regions are in the crystalline state and the gray regions are in the noncrystalline state.

In the present study, we start with considering the distribution and kinetics of the deposited atoms on the target surface. By assuming that an adatom needs on average a certain relaxation time to diffuse from the landing site to the optimal site (to continue crystalline growth) and assuming that there is an upper limit of the number of simultaneously diffusing adatoms per the surface area (to avoid collisions and agglomeration with adatoms that have not yet reached their optimal sites), we arrive at a probabilistic expression for the crystalline growth. Relating this expression to the polycrystalline ratio of the deposited poly-Si film (**Figure 2**) we obtain a formula for the polycrystalline ratio as a function of the deposition rate and size of the cell.

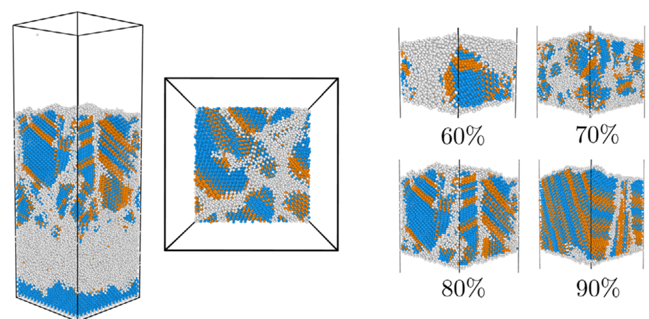

Figure 2. Left: an example of the simulation of the deposition of poly-Si: a simulation cell after the deposition and a top view of the cell after the noncrystalline part have been cut away. Right: examples of simulated poly-Si films with 60, 70, 80, and 90% polycrystalline ratio. The colored regions, cubic diamond (blue) and hexagonal diamond (orange), are crystalline grains and the gray areas are in the noncrystalline state. The simulations lead to noncrystalline parts at the bottom and top of the simulation cell. They (including the substrate at the bottom) have been removed before the polycrystalline ratio r_{pc} is calculated using the OVITO PTM method. Polycrystalline ratio r_{pc} is the ratio of the (colored) volume of the crystalline part to the total volume of the film.

© 2024 The Author(s). physica status solidi (b) basic solid state physics published by Wiley-VCH GmbH

15213951, 0, Downloaded from https://onlinelibrary.wiley.com/doi/10.1002/pssb.202400483 by Duodecim Medical Publications Ltd, Wiley Online Library on [17/01/2025]. See the Terms and Conditions (https://onlinelibrary.wiley.com/terms-and-conditions) on Wiley Online Library for rules of use; OA articles are governed by the applicable Creative Commons License

To determine the values of the parameters of the obtained formula, it is fitted to the deposition data obtained in ref. [25].

3. A Model for Controlling Polycrystalline Ratio in the Simulation of Poly-Si Film Depositions

Plotting the time interval between the successive depositions of atoms (Δt) as a function of the surface area of the simulation cell (A) for a set of fixed crystallinities (r_{pc}) (r_{pc} is calculated as the ratio of the number of atoms in the crystalline phase to the total number of atoms in the film) shows a characteristic feature for every r_{pc} (**Figure 3**). There seems to be limiting values of A and Δt. Decreasing A below the limiting value requires a significant increase in Δt, and vice versa, decreasing Δt below the limiting value requires a significant increase in A to keep the polycrystalline ratio r_{pc} at the preset value. This feature raised the question of what physics could be behind the observed phenomenon. We seek an answer to this question by examining both the kinetics of the adsorbed atoms and the probabilities of adsorption events.

3.1. Probability Analysis of the Growth

We estimate the probabilities of atomistic deposition events related to the interactions between adsorbed atoms. Let us assume the surface of the simulation cell (area A) is divided into

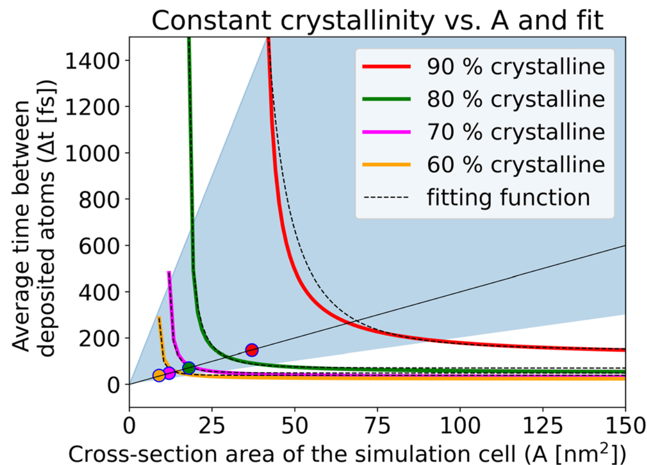

Figure 3. The data obtained from the simulations are plotted (for four fixed r_{pc}) as the time interval Δt of adatoms arriving on the surface as a function of the cross-sectional area of the simulation cell A (colored continuous curves). The dashed black curves show the fit function (Equation (8)) for each polycrystalline ratio $r_{pc} = 0.9$, 0.8, 0.7, and 0.6 (for $r_{pc} \leq 0.8$ the fit function and the simulation data practically coincide). The values of the fitting parameters Δt_0, A_0 and n are shown in Table 2. The light blue wedge is the area of recommended values for A and Δt (see Section 4). The target polycrystalline ratio r_{pc} increases continuously when moving in the direction of the opening in the blue wedge. The fitting parameters (A_0, Δt_0) for the polycrystalline ratios $r_{pc} = 0.9$, 0.8, 0.7, and 0.6 are shown by dots with the same color as the curves of the corresponding polycrystalline ratios. The fitting parameters are approximately on the line $\Delta t = c \times A$, $c = 4\,\text{fs nm}^{-2}$. The effect of temperature on the polycrystalline ratio of $A = 36\,\text{nm}^2$, $\Delta t = 250$ fs film is shown in Figure 1.

smaller subcells (area A_0). From the point of view of crystallization, it is disadvantageous if several adatoms are adsorbed in the same subcell within a short time. For instance, the activation energy of a single-adatom diffusion on Si(001) is 0.67 eV whereas for a Si dimer it is 1.09 eV along the dimer row and 0.70 and 1.36 eV double barrier across the dimer row.[40,41] Although in our case the surface consists of grains with different crystal orientations and noncrystalline grain boundaries between the grains, and in addition, the surface is under constant bombardment of adatoms, the essential point is that the diffusion of a group of adatoms is slower than the diffusion of a single adatom. Therefore, from the point of view of crystalline growth, it is advantageous that no more adsorbate atoms are added to A_0 before the previous adsorbate adatoms have had time to diffuse to energetically favorable crystal positions.

When a subcell has newly adsorbed atoms, it needs a certain time (t_{rel}) without further adsorptions for crystallization to occur. The probability that n consecutive adatoms are adsorbed in the same subcell is $(A_0/A)^n$. The probability that this will not happen (a beneficial case concerning the crystallization, no clumps of adatoms) is

$$P_1 = 1 - (A_0/A)^n \tag{5}$$

During time t_{rel}, $t_{rel}/\Delta t$ atoms are adsorbed on the surface and the probability that no n consecutive adatoms are adsorbed in the same subcells is

$$P_2 = P_1^{(t_{rel}/\Delta t)/n} = [1 - (A_0/A)^n]^{t_{rel}/(n\Delta t)} \tag{6}$$

In our case $\Delta t > 0$ because otherwise there will be no crystalline growth. Implementing the lower limit (Δt_0) of Δt into the exponent in P_2 by shifting the origin as follows $\Delta t \rightarrow \Delta t - \Delta t_0$, assuming $t_{rel}/n \approx \Delta t_0$, and equating the probability P_2 with the target polycrystalline ratio r_{pc} leads to Equation (7):

$$[1 - (A_0/A)^n]^{\frac{\Delta t_0}{\Delta t - \Delta t_0}} = r_{pc} \tag{7}$$

We see that the exponent has the correct limiting values:

$$(i)\ \frac{\Delta t_0}{\Delta t - \Delta t_0} \rightarrow \infty, \text{ when } \Delta t \rightarrow \Delta t_0$$

$$(ii)\ \frac{\Delta t_0}{\Delta t - \Delta t_0} \rightarrow 0, \text{ when } \Delta t \rightarrow \infty$$

Case (i) means that probability $P_2 \rightarrow 0$ and in the deposition there are only few subcells having n or less simultaneous unrelaxed adatoms (low polycrystalline ratio expected). Case (ii) means that probability $P_2 \rightarrow 1$ and in the deposition there are many subcells having n or less simultaneous unrelaxed adatoms (high polycrystalline ratio expected). Taking the logarithm of both sides of Equation (7) leads to Equation (8):

$$\Delta t = \Delta t_0 \frac{\ln[1 - (A_0/A)^n]}{\ln(r_{pc})} + \Delta t_0 \tag{8}$$

where the parameters n, Δt_0, and A_0 are to be fitted to the (A, Δt, r_{pc}) data from simulations (ref. [25]).

© 2024 The Author(s). physica status solidi (b) basic solid state physics published by Wiley-VCH GmbH

15213951, 0, Downloaded from https://onlinelibrary.wiley.com/doi/10.1002/pssb.202400483 by Duodecim Medical Publications Ltd, Wiley Online Library on [17/01/2025]. See the Terms and Conditions (https://onlinelibrary.wiley.com/terms-and-conditions) on Wiley Online Library for rules of use; OA articles are governed by the applicable Creative Commons License

15213951, 0, Downloaded from https://onlinelibrary.wiley.com/doi/10.1002/pssb.202400483 by Duodecim Medical Publications Ltd, Wiley Online Library on [17/01/2025]. See the Terms and Conditions (https://onlinelibrary.wiley.com/terms-and-conditions) on Wiley Online Library for rules of use; OA articles are governed by the applicable Creative Commons License

3.2. Fitting the Model to the Poly-Si Deposition Simulation Data

Deposition is a method based on atomistic random processes for the fabrication of thin films. This also causes random variations in the end products. It is therefore challenging to perform simulations that produce poly-Si films with a predetermined precise polycrystalline ratio. To overcome this, we performed several simulations with different growth conditions and used the resulting dataset of $(A, \Delta t, r_{pc})$ triplets to estimate A and Δt for films with polycrystalline ratios $r_{pc} = 0.9$, 0.8, 0.7, and 0.6. This was done in our previous work[25] where we found that the polycrystalline ratio Function (9) (note, in Function (9) polycrystalline ratio is in %) represents well the simulated data. Here, we use the Function (9) to extract the $(A, \Delta t)$ data for fixed r_{pc} values:

$$K(A, \Delta t) = -\frac{315.3\,\text{nm}^2}{A} - \frac{882.6\,\text{fs}}{\Delta t} + 98.09 \quad [\%] \tag{9}$$

The 3D map of the polycrystalline ratio $K(A, \Delta t)$ as a function of A and Δt is shown in **Figure 4**.

The function, shown in Equation (9) and in Figure 4, is based on the data from 36 deposited poly-Si films. The polycrystalline ratio was determined by OVITO using the PTM method, which gives the number of atoms in the crystalline and noncrystalline phases of the film. The height curves corresponding to the crystallinities $r_{pc} = 0.9$, 0.8, 0.7, and 0.6 are also shown on the plotted $K(A, \Delta t)$ surface in Figure 4. On the bottom plane are the projections of the height curves, which are also shown in Figure 3.

The $(A, \Delta t)$ data from function 9 are then used to fit the Function (8) for the polycrystalline ratios $r_{pc} = 0.9$, 0.8, 0.7, and 0.6. The fitted functions are shown in Figure 3 (black dashed curves) and the fitted values of the parameters Δt_0 and A_0 are shown in **Table 2**. The $n = 4$ leads to the best fit to the simulated data for every r_{pc}. Fitting is done using the curve_fit function from Python library SciPy.[39] The ratio $A_0/\Delta t_0$ is almost constant over different polycrystalline ratios.

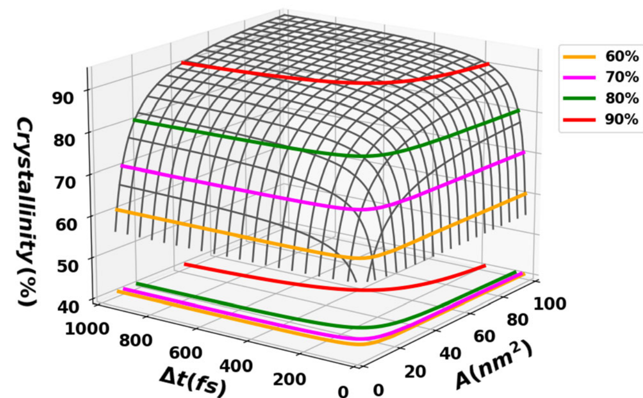

Figure 4. Plot of the function $K(A, \Delta t)$ (Equation (9)). The figure shows the cutting curves of the function $K(A, \Delta t)$ and the constant polycrystalline ratio planes $r_{pc} = 0.9$, 0.8, 0.7, and 0.6, as well as the projections of the cutting curves onto the base plane (these are the curves shown also in Figure 3).

Table 2. The values of the fitted parameters Δt_0 and A_0 (Function (8)) for polycrystalline ratios $r_{pc} = 0.9$, 0.8, 0.7, and 0.6.

r_{pc} [a]	Δt_0 [fs]	A_0 [nm^2]	$A_0/\Delta t_0$ [nm^2 fs^{-1}]
0.9	147.5	37.3	0.25
0.8	70.8	18.0	0.25
0.7	49.2	11.9	0.23
0.6	39.3	8.9	0.23

[a] The optimum value of the parameter n is 4. The ratio $A_0/\Delta t_0$ is almost constant.

The fitted parameter pairs $(A_0, \Delta t_0)$ for different r_{pc} values are shown in Figure 3. The points are approximately on the straight line, which means that interpolation or extrapolation of the parameters to any target polycrystalline ratio can be done conveniently with a linear function.

Considering random walk statistics suggests a relation between A_0 and Δt_0. With the assumption that there are only nearest-neighbor jumps, according to the random walk statistics the ratio $\langle \Delta r^2 \rangle / t = a^2\Gamma$. $a^2\Gamma$ is constant at constant temperature and $\langle \Delta r^2 \rangle$, t, a, and Γ are the mean squared displacement of an atom, the diffusing time, the jump distance, and the jump rate, respectively.[42] Comparing our result $A_0/\Delta t_0 \approx$ constant (Table 2) with the above random walk result suggests that the basic parameters A_0 and Δt_0 are related to fundamental diffusion parameters.

4. Interpretation of the Results

4.1. Optimal Flux

To interpret the results, let us first take a closer look at two features of molecular dynamics simulations of the deposition processes. The flux Φ of atoms deposited on the surface depends on the surface area A and the average atom import frequency $1/\Delta t$ to the surface, $\Phi = 1/(\Delta t A)$. As our simulations show, the level of polycrystalline ratio of the deposited poly-Si film depends on the flux, but not only on the flux. Especially in cases where the target polycrystalline ratio of the poly-Si film is lower than 80%, the flux is not the determining factor for the level of polycrystalline ratio.

When a deposited atom comes to the surface, the first adsorption site is most likely not the most energetically optimal site for it. Therefore, the adatom diffuses some distance from its first adsorption site over some time before it finds the optimal low-energy adsorption site. If the deposition flux is high, it is possible that other atoms are deposited close to the first one and the deposited atoms form a clump that locks onto the surface at a point that might not be optimal for subsequent crystallization. These features are to some extent captured in the Functions (8) and (7) with the parameters A_0, Δt_0, and n.

Fitting the Function (8) to the simulation data leads to the values of A_0 and Δt_0 shown in Table 2. When the target polycrystalline ratio of the deposited poly-Si film decreases, both A_0 and Δt_0 decrease accordingly. This can be understood in the following way: as the target polycrystalline ratio decreases, a smaller

© 2024 The Author(s). physica status solidi (b) basic solid state physics published by Wiley-VCH GmbH

area and a shorter time interval (a higher probability of forming clumps is allowed) are still sufficient to produce a poly-Si film with the required polycrystalline ratio. The optimal value of the parameter n is 4 regardless of the target polycrystalline ratio. This can be understood as parameters A_0 and Δt_0 already include the major effects of the change in the target polycrystalline ratio.

As Figure 3 shows, the fit is not perfect for the $r_{pc} = 0.9$. The curvature of the simulation data at about $A = 50\,\text{nm}^2$ is higher than the curvature of the fit function. This is because the fit Function (8) approaches 100% crystallinity when A and Δt approach infinity whereas the extrapolation from the simulation data leads to 98% polycrystalline ratio. However, the 100% crystallinity is irrelevant in our case because we are interested in poly-Si, which in any case contains noncrystalline grain boundaries.

Figure 5 shows the deposition flux Φ as a function of the surface area A of the simulation cell for four target polycrystalline ratio. $\Phi(A) = 1/(\Delta t A)$, where $\Delta t = \Delta t(A)$, for each fixed r_{pc}, as shown in Figure 3.

All the $\Phi(A)$ curves have the maximum at $A \approx 2A_0$. There are two different poly-Si deposition regions separated by Φ_{max}. When $A < 2A_0$, the crystallization of Si strongly depends on the simulation cell size which can, however, be compensated with changing the flux Φ (i.e., Δt). The hard limit for each polycrystalline ratio (r_{pc}) is $A = A_0(r_{pc})$, below which the growth of poly-Si is not possible. In the range $A > 2A_0$, as A increases, the size of the simulation cell limits crystallization less and less. For large A, the polycrystalline ratio is determined mainly by the flux. Although the polycrystalline ratio remains constant in the curves of Figure 5, it is expected that the grain size and shape distributions will change. However, a more detailed study of this would require a considerable number of simulations, to achieve reliable statistics, which was not possible.

The value of Φ_{max} increases with decreasing target polycrystalline ratio. The reason is that as the target polycrystalline ratio decreases, the $\Delta t = \Delta t(A)$ curves (Figure 3) shift lower and extend to smaller A values with smaller Δt, which increases Φ.

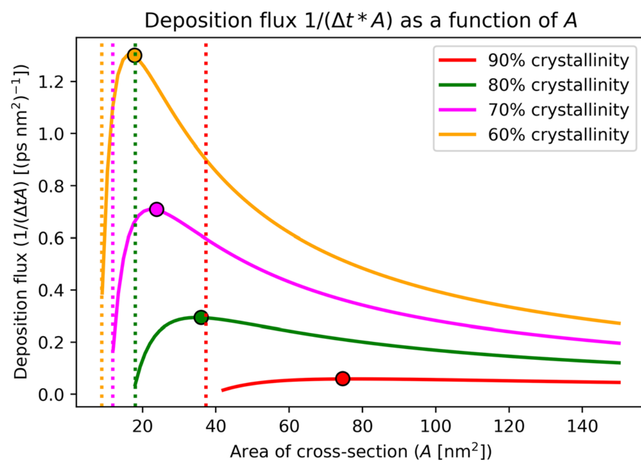

Figure 5. Deposition flux $(1/(\Delta t A))$ as a function of A for polycrystalline ratios $r_{pc} = 0.9,\ 0.8,\ 0.7,$ and 0.6 (the lower the polycrystalline ratio, the higher the corresponding curve locates). The vertical dotted lines show the positions of A_0 (Table 2). The flux for each r_{pc} at $2A_0$ is shown with a dot in the color of the curve.

However, moving to even smaller A values, the deposition flux drops very steeply for 60, 70, and 80% polycrystalline ratio cases. This is due to the sharply increasing Δt compensating the very small A values (Figure 3). In the case of 60% polycrystalline ratio, the maximum possible deposition flux is about 4 times the smallest deposition flux, while in the case of 90% polycrystalline ratio, the deposition flux does not vary much. In cases of high-target polycrystalline ratio, the deposition conditions are more stringent than in cases of low polycrystalline ratio, limiting the possible (Δt, A) values in the case of 90% polycrystalline ratio.

If the target polycrystalline ratio in simulations is lower than 80%, it would be beneficial to use Equation (8) to estimate the optimal combination (Δt, A) to use the highest possible flux (shortest computational time) to save computational resources in simulations, which is a great advantage if a large number of simulations are required.

To explain the shapes of the curves shown in Figure 5, it is necessary to consider the physics behind the deposition parameters. A key issue arises when comparing poly-Si deposition simulations with different-sized simulation cells. Let the cross-sectional areas of the cells in two simulations (1 and 2) be denoted as A_1 and A_2. If $A_1 = \alpha A_2$, where $\alpha > 1$, the fluxes in both cases are equivalent if the time durations are related as $\Delta t_2 = \alpha \Delta t_1$. However, equal fluxes do not imply identical physics in simulations since the probability of the two successive deposited atoms landing near each other (denoted as P_{cl}) differs between the two systems.

For a given time period t, $\Delta t_1 < t < \Delta t_2$, the probability of close landing in simulation 2 is $P_{cl} = 0$ while in simulation 1 it is $P_{cl} \neq 0$. To maintain more similar physics between the two simulations, the flux must be increased in simulation 2 (which has a smaller cross-sectional area A). This explains why the fixed r_{pc} curves rise when the simulation cell cross section (A) decreases. This trend continues until the cross-sectional area A becomes sufficiently small (at point $2A_0$ in Figure 5) at which point there is not enough space in the simulation cell to receive the required r_{pc} at such a high flux and the flux starts to drop for $A < 2A_0$.

For lower r_{pc} values, this flux reduction occurs at smaller A values, as lower r_{pc} allows for more misplaced atoms in poly-Si. Since $r_{pc} = 0.9$ is a stringent requirement, the flux is constrained to lower values over a wide range of A.

Thermodynamically, the crystallization of Si can be studied with the Gibbs free energy G.

$$G = U - TS + PV \tag{10}$$

where U, T, S, P, and V are internal energy, temperature, entropy, pressure, and volume of the considered system, respectively. The ground state (crystalline) of Si corresponds to minimum Gibbs free energy of Si. The production of polysilicon, on the other hand, is a nonequilibrium process, resulting in a material that is only partially crystallized due to kinetic restrictions. In our simulations, the restriction on crystallization is determined by the area of the simulation cell (A) and the time interval between successive atom depositions (Δt). Mathematically, this is expressed in Equation (7), which connects A, Δt, and r_{pc}. Graphically their relation is shown in Figure 5.

© 2024 The Author(s). physica status solidi (b) basic solid state physics published by Wiley-VCH GmbH

15213951, 0, Downloaded from https://onlinelibrary.wiley.com/doi/10.1002/pssb.202400483 by Duodecim Medical Publications Ltd, Wiley Online Library on [17/01/2025]. See the Terms and Conditions (https://onlinelibrary.wiley.com/terms-and-conditions) on Wiley Online Library for rules of use; OA articles are governed by the applicable Creative Commons License

15213951, 0, Downloaded from https://onlinelibrary.wiley.com/doi/10.1002/pssb.202400483 by Duodecim Medical Publications Ltd, Wiley Online Library on [17/01/2025]. See the Terms and Conditions (https://onlinelibrary.wiley.com/terms-and-conditions) on Wiley Online Library for rules of use; OA articles are governed by the applicable Creative Commons License

The Gibbs energy minimization with constraints can be done using the method of Lagrange undetermined multipliers.[43]

In the present case, the constraint function is $g = N_c/(N_c + N_n) - r_{pc}$, where N_c and N_n are the number of atoms in the crystalline and noncrystalline phases, respectively, and r_{pc} is obtained from Equation (8). The final state of the system is obtained by minimizing the Lagrangian $L = G + \lambda g$ by solving its stationary points as the zero points of its partial derivatives, $\frac{\partial L}{\partial N_c} = \frac{\partial L}{\partial N_n} = \frac{\partial L}{\partial \lambda} = 0$.

4.2. Geometric Consideration

A geometric study of the poly-Si surface can also provide useful information. Since polysilicon tends to consist of needle shape grains perpendicular to the growth surface, we model poly-Si films as consisting of beam-like grains, oriented perpendicular to the surface. We first consider grains of equal-sized square shape cross-sectional area (**Figure 6**). The square cross-sectional area of the grains at the surface is $A = L^2$ and the thickness of the grain boundaries is d. (In this subsection, A refers to the cross-sectional area of the grain, not the area of the simulation cell, as before.) The grains are assumed to be crystalline and the grain boundaries between the grains are noncrystalline. We fix the polycrystalline ratio of the film ($r_{pc} = A/A_{tot}$, $A_{tot} = A + A_d$, where A_d is the grain boundary area belonging to one grain). Within this approximation, d is given by

$$d = \left(1 - \sqrt{r_{pc}}\right)\sqrt{A_{tot}} \quad (11)$$

Plotting d as a function of A_{tot} for crystallinities $r_{pc} = 0.6$, 0.7, 0.8, and 0.9 yields a series of square-root type curves. The four thinnest grain boundary thicknesses obtained in the simulations of poly-Si[26] are shown with dashed horizontal lines in Figure 6.

According to the geometric model (Equation (11)), as the surface area (A_{tot}) decreases, the grain boundary thickness (d) also decreases, provided the polycrystalline ratio (r_{pc}) is kept constant. Since the crystal directions of adjacent grains are not coherent, grain boundary thinning becomes more difficult as the grain boundary thins. According to our simulations, the lower limit of the grain boundary thickness is 0.46 nm.[26] To get very thin grain boundaries in simulations of poly-Si depositions the rate of deposition should be decreased, i.e., Δt should be increased. This effect can be seen in Figure 3 as a sharp increase in Δt while reducing the size of the simulation cell.

As the size of the simulation cell decreases, the maximum grain size also decreases because matching a multiple of the Si lattice parameter to the size of the simulation cell becomes more challenging. Thus, the square grain model (Equation (11)) is in line with the following three features observed in Figure 3: 1) Δt starts to increase in the order of $r_{pc} = 0.9$, 0.8, 0.7, and 0.6. As shown in Figure 6, the d-curves (Equation (11)) cross the four dashed lines of the smallest grain boundary thicknesses (0.46, 0.61, 0.79, and 0.95 nm)[26] in the order of decreasing r_{pc}; 2) The rise of Δt gets steeper with decreasing r_{pc} because the d-curves in Figure 6 sweep in a more and more steeply manner through the horizontal dashed lines with decreasing r_{pc}; 3) The distance between successive Δt rising points in the A-axis shortens when going to smaller A values. This is due to the increasing slope of the d-curves near the point $A_{tot} = 0$ as the polycrystalline ratio r_{pc} decreases (Figure 6).

Next, we investigate a few other grain shapes to show that the result obtained for the square grain model is not a special case but a manifestation of a general geometric-dimensional phenomenon.

First, we present a theorem related to the thickness of the grain boundary and the total area of the grain and grain boundary for tessellations of the surface: If there is a quantity X and real numbers α, β, and γ such that the area A of a grain is $A = \alpha X^2$ and the combined area A_{tot} of the grain and the grain boundary is $A_{tot} = \gamma(X + \beta d)^2$, where d is the grain boundary thickness, then d and A_{tot} are related as (see Supporting Information for proof)

$$d = \frac{1}{\beta\sqrt{\alpha}}\left(\sqrt{\frac{\alpha}{\gamma}} - \sqrt{r_{pc}}\right)\sqrt{A_{tot}} \quad (12)$$

Based on Equation (12), the functions $d = d(A_{tot})$ for rhombi, equilateral triangles, and regular hexagons are shown in Equation (13). Equation (12) does not apply to circles because

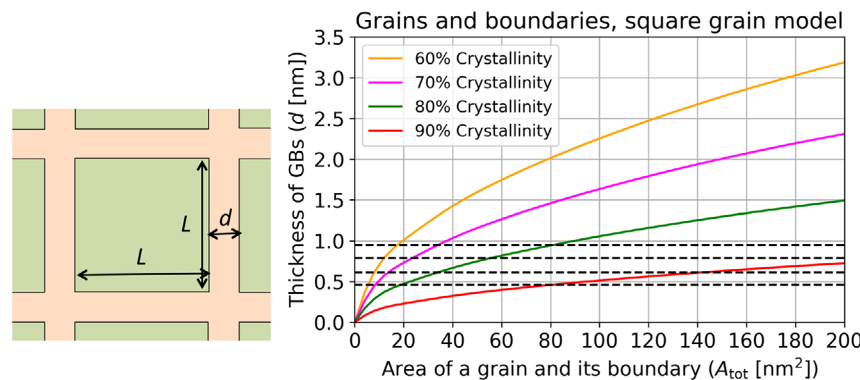

Figure 6. Left: schematic of the square grain model. The surface cross-sectional area of the grains is L^2 and the thickness of the grain boundaries is d. Right: The grain boundary thickness (d) as a function of the surface area (A_{tot}) for the polycrystalline ratios $r_{pc} = 0.6$, 0.7, 0.8, and 0.9. The four horizontal dashed lines show the values of the four thinnest possible grain boundaries[26] found in the simulations of the deposition of polycrystalline Si, 0.46, 0.61, 0.79, and 0.95 nm.

© 2024 The Author(s). physica status solidi (b) basic solid state physics published by Wiley-VCH GmbH

15213951, 0, Downloaded from https://onlinelibrary.wiley.com/doi/10.1002/pssb.202400483 by Duodecim Medical Publications Ltd, Wiley Online Library on [17/01/2025]. See the Terms and Conditions (https://onlinelibrary.wiley.com/terms-and-conditions) on Wiley Online Library for rules of use; OA articles are governed by the applicable Creative Commons License

it is impossible to tile a surface by circles seamlessly. The outcome is expected, as the cross-sectional area of the grain boundary is proportional to the length of the grain circumference, which, in turn, is proportional to the square root of the cross-sectional area of the grain.

$$\begin{aligned} d &= \sqrt{\sin\theta}\left(1-\sqrt{r_{\text{pc}}}\right)\sqrt{A_{\text{tot}}} \text{ (rhombus with an angle } \theta) \\ d &= \sqrt{\tfrac{4}{3\sqrt{3}}}\left(1-\sqrt{r_{\text{pc}}}\right)\sqrt{A_{\text{tot}}} \text{ (equilateral triangle)} \\ d &= \sqrt{\tfrac{2}{\sqrt{3}}}\left(1-\sqrt{r_{\text{pc}}}\right)\sqrt{A_{\text{tot}}} \text{ (regular hexagon)} \\ d &= \tfrac{2}{\sqrt{3\pi}}\left(\sqrt{\tfrac{\pi}{2\sqrt{3}}}-\sqrt{r_{\text{pc}}}\right)\sqrt{A_{\text{tot}}} \text{ (circle)} \end{aligned} \tag{13}$$

The square case, discussed at the beginning of this subsection, is a special case of rhombi with an angle $\theta = 90$. The coefficient $\sqrt{\sin\theta}$ of the term $\left(1-\sqrt{r_{\text{pc}}}\right)$ reflects the ratio of the volume to the circumference of a polygon. When this ratio becomes smaller, the cofactor decreases. The cofactors of equilateral triangles, squares, and regular hexagons, $\sqrt{4/(3\sqrt{3})} \leq 1 \leq \sqrt{2/\sqrt{3}}$, increase with the area to the circumference ratio. The grain boundary area of circles, consisting of the pockets between the circles, reaches a finite value when the circles approach each other. This is why, in the case of circles, the constant term in parentheses is $\sqrt{\pi/(2\sqrt{3})}$ instead of 1.

Considering the grain boundary thickness curves in Figure 6, the whole set of curves shifts down for equilateral triangles and up for regular hexagons, as compared with that of squares. It should also be noted that the average d of the mixture of different grain shapes scales like $\sqrt{A_{\text{tot}}}$ in line with the model presented above.

If the grain size distribution is known, the obtained grain boundary thickness results can also be used to analyze poly-Si surfaces with different size grains. For instance, the average grain boundary thickness $\overline{d}$ is obtained by integrating the grain size distribution with the grain boundary thickness function (Equation (11) or (13)):

$$\overline{d}(r_{\text{pc}}) = \int_0^{A_{\max}} d(A, r_{\text{pc}}) f(A)\text{d}A \tag{14}$$

where $d(A, r_{\text{pc}})$ is the grain boundary thickness and $f(A)$ is the grain size distribution. In many cases, the log-normal distribution $f(x) = \exp(-(\ln(x)-\mu)/\sigma)^2/2)/(x\sigma\sqrt{2\pi})$ is a good approximation for the grain size distribution. In $f(x)$, μ and σ are the location and scale parameters. Using $\mu = 3$, $\sigma = 1$ (log-normal distribution with mean 33), and $r_{\text{pc}} = 0.8$ results in $\overline{d} = 0.58$ nm, which is close to the grain boundary thickness of a homogeneous distribution of 33 nm^2 square grains in the case of $r_{\text{pc}} = 0.8$ (Figure 6).

5. Conclusion

The constructed deposition model (Equation (8)) was fitted to the data of 36 simulated depositions of poly-Si films. The physical interpretation of the fitting parameters of the model can pave the way for more precise control of poly-Si film growth. Our main findings are listed below. 1) The ranges of the size of the simulation cell (A) and the deposition period (Δt) for the efficient (high flux) simulation of the deposition of poly-Si films (Figure 3 and 5) were obtained; 2) The function $\Delta t = \Delta t(A, r_{\text{pc}})$, containing physically transparent parameters Δt_0 and A_0 (Equation (8)), can be used as a guide to select the correct Δt and A to simulate poly-Si with specified polycrystalline ratio; 3) The simulation cell size of about $A = 10\,\text{nm}^2$ seems to be so small that films containing crystallites cannot be achieved at any Δt. This can be linked to the cell size limit where crystallite growth is inhibited; 4) The physical meaning of the parameters A_0 and Δt_0 of the poly-Si growth model (Equation (8)) has been clarified. The parameter A_0 reflects the size of the smallest possible simulation cell that can be used in poly-Si growth simulations. The geometric consideration reveals that parameter Δt_0 has connection to the lower limit of the grain boundary thickness of poly-Si; 5) The illustrative geometric model (Equation (13) and Figure 6) explains qualitatively the main features observed in the simulations of the deposition of poly-Si.

Supporting Information

Supporting Information is available from the Wiley Online Library or from the author.

Acknowledgements

The work was supported by the Business Finland (project BEETLES TY 1320731/2021) and Okmetic Oy. The computer resources of the Finnish IT Center for Science (CSC) and the Finnish Computing Competence Infrastructure (FCCI) project (Finland) are acknowledged.

Conflict of Interest

The authors declare no conflict of interest.

Data Availability Statement

The data that support the findings of this study are available from the corresponding author upon reasonable request.

Keywords

crystal growth, crystallinity, deposition models, deposition of thin films, grain boundaries, molecular dynamics simulations, polycrystalline silicon

Received: September 12, 2024
Revised: November 28, 2024
Published online:

[1] T. I. Kamins, in *Polycrystalline Silicon for Integrated Circuits and Displays*, Kluver Academic Publishers, Dordrecht **1998**.
[2] E. S. Kenu, R. Uhunmwangho, E. N. C. Okafor, *Int. J. Eng. Res. Technol.* **2020**, *9*, 741.
[3] R. J. Ram, *SPIE Proc.* **2015**, *9367*, 93670N1.
[4] P. J. French, *Sens. Actuators, A* **2002**, *99*, 3.

© 2024 The Author(s). physica status solidi (b) basic solid state physics published by Wiley-VCH GmbH

15213951, 0, Downloaded from https://onlinelibrary.wiley.com/doi/10.1002/pssb.202400483 by Duodecim Medical Publications Ltd, Wiley Online Library on [17/01/2025]. See the Terms and Conditions (https://onlinelibrary.wiley.com/terms-and-conditions) on Wiley Online Library for rules of use; OA articles are governed by the applicable Creative Commons License

[5] S. Jagar, M. Chan, H. Wang, V. M. C. Poon, A. M. Myasnikov, *Solid-State Electron.* **2001**, *45*, 743.
[6] A. Polyakov, S. Sinaga, P. M. Mendes, M. Bartek, J. H. Correia, J. N. Burghartz, *Electron. Lett.* **2005**, *41*, 100.
[7] A. B. Siddique, K. A. Rahman, M. N. Alam, K. Hasan, M. M. A. Hakim, in *2018 10th Int. Conf. on Electrical and Computer Engineering (ICECE)*, Dhaka Bangladesh **2018**, pp. 213–216.
[8] J. K. Rath, *Sol. Energy Mater. Sol. Cells* **2003**, *76*, 431.
[9] K. Wu, J. Cheng, G. Huang, J. Yuan, K. Xu, *Opt. Mater.* **2020**, *102*, 109783.
[10] K.-H. Jang, *PhD Thesis: Evaluation of Thermal Annealing Before and After Formation of Gate Insulator Films by Extracting Trap Densities for SPC Poly-Si TFTs*, Department of Electrical Engineering and Information Systems, University of Tokyo **2020**.
[11] J. Pyo, B. Lee, H.-Y. Ryu, *Micromachines* **2021**, *12*, 999.
[12] D. C. Moschou, M. Exarchos, D. N. Kouvatsos, G. J. Papaioannou, A. T. Voutsas, *Microelectron. Reliab.* **2007**, *47*, 1378.
[13] L. Gránásy, T. Pusztai, J. A. Warren, *J. Phys.: Condens. Matter* **2004**, *16*, R1205.
[14] A. Baiano, R. Ishihara, J. van der Cingel, K. Beenakker, *IEEE Electron Device Lett.* **2010**, *31*, 308.
[15] J. H. Ahn, B. T. Ahn, *J. Electrochem. Soc.* **2001**, *148*, H115.
[16] M. S. Haque, H. A. Naseem, W. D. Brown, *J. Appl. Phys.* **1994**, *75*, 3928.
[17] Y. Ebiko, K. Suzuki, N. Sasaki, *IEEE Trans. Electron Devices* **2005**, *52*, 429.
[18] V. Subramanian, P. Dankoski, L. Degertekin, B. T. Khuri-Yakub, K. C. Saraswat, *IEEE Electron Device Lett.* **1997**, *18*, 378.
[19] M. Kimura, Y. Hiroshima, *IEEE Electron Device Lett.* **2013**, *34*, 256.
[20] M.-H. Weng, C.-T. Cheng-Tang Pan, C.-W. Huang, R.-Y. Yang, *J. Nanomater.* **2014**, *2014*, 342478.
[21] M. Rack, F. Allibert, J.-P. Raskin, *IEEE Trans. Electron Devices* **2021**, *68*, 4598.
[22] M. Rack, F. Allibert, J.-P. Raskin, *IEEE Trans. Electron Devices* **2021**, *68*, 4606.
[23] L. Ding, J.-P. Raskin, G. Lumbeeck, D. Schryvers, H. Idrissi, *Mater. Charact.* **2020**, *161*, 110174.
[24] A. Poruba, A. Fejfar, Z. Remeš, J. Špringer, M. Vaněček, J. Kočka, J. Meier, P. Torres, A. Shah, *J. Appl. Phys.* **2000**, *88*, 148.
[25] M. Santonen, A. Lahti, Z. J. Rad, M. Miettinen, M. Ebrahimzadeh, J.-P. Lehtiö, P. Laukkanen, M. Punkkinen, P. Paturi, K. Kokko, A. Kuronen, W. Li, L. Vitos, K. Parkkinen, M. Eklund, *Modell. Simul. Mater. Sci. Eng.* **2024**, *32*, 065025.
[26] A. Lahti, M. Santonen, Z. J. Rad, M. Miettinen, M. Ebrahimzadeh, J.-P. Lehtiö, P. Laukkanen, M. Punkkinen, P. Petriina, K. Kokko, A. Kuronen, W. Li, L. Vitos, K. Parkkinen, M. Eklund, *Modell. Simul. Mater. Sci. Eng.* **2024**, *32*, 065026.
[27] A. P. Thompson, H. M. Aktulga, R. Berger, D. S. Bolintineanu, W. M. Brown, P. S. Crozier, P. J. in't Veld, A. Kohlmeyer, S. G. Moore, T. D. Nguyen, R. Shan, M. J. Stevens, J. Tranchida, C. Trott, S. J. Plimpton, *Comput. Phys. Commun.* **2022**, *271*, 108171.
[28] T. A. Weber, F. H. Stillinger, *Phys. Rev. B* **1985**, *31*, 1954.
[29] J. Tersoff, *Phys. Rev. B* **1988**, *37*, 6991.
[30] T. Kumagai, S. Izumi, S. Hara, S. Sakai, *Comput. Mater. Sci.* **2007**, *39*, 457.
[31] G. P. Pun, Y. Mishin, *Phys. Rev. B* **2017**, *95*, 224103.
[32] J. F. Justo, M. Z. Bazant, E. Kaxiras, *Phys. Rev. B* **1998**, *58*, 2539.
[33] T. J. Lenosky, B. Sadigh, E. Alonso, V. V. Bulatov, T. Diaz De La Rubia, J. Kim, A. F. Voter, J. D. Kress, *Modell. Simul. Mater. Sci. Eng.* **2000**, *8*, 825.
[34] Y. A. Du, T. J. Lenosky, R. G. Hennig, S. Goedecker, J. W. Wilkins, *Phys. Status Solidi* **2011**, *248*, 2050.
[35] Y. Zuo, C. Chen, X. Li, Z. Deng, Y. Chen, J. Behler, G. Csányi, A. V. Shapeev, A. P. Thompson, M. A. Wood, S. P. Ong, *J. Phys. Chem. A* **2020**, *124*, 731.
[36] P. Hirel, *Comput. Phys. Commun.* **2015**, *197*, 212.
[37] P. M. Larsen, S. Schmidt, J. Schiøtz, *Modell. Simul. Mater. Sci. Eng.* **2016**, *24*, 055007.
[38] A. Stukowski, *Modell. Simul. Mater. Sci. Eng.* **2010**, *18*, 015012.
[39] P. Virtanen, R. Gommers, T. E. Oliphant, M. Haberland, T. Reddy, D. Cournapeau, E. Burovski, P. Peterson, W. Weckesser, J. Bright, S. J. van der Walt, M. Brett, J. Wilson, K. J. Millman, N. Mayorov, A. R. J. Nelson, E. Jones, R. Kern, E. Larson, C. J. Carey, I. Polat, Y. Feng, E. W. Moore, J. VanderPlas, D. Laxalde, J. Perktold, R. Cimrman, I. Henriksen, E. A. Quintero, C. R. Harris, et al., *Nat. Methods* **2020**, *17*, 261.
[40] Y. W. Mo, J. Kleiner, M. B. Webb, M. G. Lagally, *Surf. Sci.* **1992**, *268*, 275.
[41] B. Borovsky, M. Krueger, E. Ganz, *Phys. Rev. Lett.* **1997**, *78*, 4229.
[42] A. G. Naumovets, Y. S. Vedula, *Surf. Sci. Rep.* **1985**, *4*, 365.
[43] P. Koukkari, *Introduction to Constrained Gibbs Energy Methods in Process and Materials Research*, VTT Technical Research Centre of Finland **2014**, ISBN 978-951-38-8134-4.

© 2024 The Author(s). physica status solidi (b) basic solid state physics published by Wiley-VCH GmbH